AIP | Physics of Plasmas

Numerical modeling of radiation-dominated and quantum-electrodynamically strong regimes of laser-plasma interaction

Igor V. Sokolov, Natalia M. Naumova, and John A. Nees

Citation: Phys. Plasmas **18**, 093109 (2011); doi: 10.1063/1.3638138
View online: http://dx.doi.org/10.1063/1.3638138
View Table of Contents: http://pop.aip.org/resource/1/PHPAEN/v18/i9
Published by the AIP Publishing LLC.

Numerical modeling of radiation-dominated and quantum-electrodynamically strong regimes of laser-plasma interaction

Igor V. Sokolov,[1,a)] Natalia M. Naumova,[2] and John A. Nees[3]
[1]*Space Physics Research Laboratory, University of Michigan, Ann Arbor, Michigan 48109, USA*
[2]*Laboratoire d'Optique Appliquée, UMR 7639 ENSTA, Ecole Polytechnique, CNRS, 91761 Palaiseau, France*
[3]*Center for Ultrafast Optical Science and FOCUS Center, University of Michigan, Ann Arbor, Michigan 48109, USA*

(Received 9 March 2011; accepted 20 July 2011; published online 30 September 2011)

Ultra-strong laser pulses can be so intense that an electron in the focused beam loses significant energy due to γ-photon emission while its motion deviates via the radiation back-reaction. Numerical methods and tools designed to simulate radiation-dominated and quantum-electrodynamically strong laser-plasma interactions are summarized here. © *2011 American Institute of Physics*. [doi:10.1063/1.3638138]

I. INTRODUCTION

Progress in laser technologies has resulted in the opportunity to create ultra-strong electromagnetic fields in tightly focused laser beams. In the present paper, we discuss the numerical methods designed to simulate processes in strong pulsed laser fields interacting with plasma. Attention is paid to the recently achieved range of intensities, $J \geq 2 \cdot 10^{22}$ W/cm^2,[1] and the larger intensities projected, $J \sim 10^{25}$ W/cm^2.[2]

For a typical laser wavelength, $\lambda \sim 1$ μm, electron motion in laser fields at $J \geq 10^{18}$ W/cm^2 is relativistic,

$$|\mathbf{a}| \gg 1, \qquad \mathbf{a} = \frac{e\mathbf{A}}{m_e c^2}, \tag{1}$$

where m_e and $e = -|e|$ are the mass and the electric charge of an electron, respectively.

However, if we want to evaluate the properties of an electron in a strong field as an *emitting* particle moreover, a particle, which emits *photons*; we need to be guided by the more severe condition

$$|\mathbf{a}|_\alpha = \alpha|\mathbf{a}| \geq 1, \tag{2}$$

in which the fundamental fine structure constant is present, $\alpha = e^2/(c\hbar) \approx 1/137$, linking its radiation to its motion (herewith, the subscript α denotes the dimensionless parameter multiplied by α). With the recently achieved intensity of $J \sim 2 \cdot 10^{22}$ W/cm$^2 \sim (1/\alpha^2) \cdot 10^{18}$ W/cm^2, this newly important dimensionless parameter exceeded unity!

However, this estimate could be applicable only to a "theoretical laser," for which the photon energy, $\hbar\omega$, would be comparable to the "characteristic" atomic unit (au) of energy, $2\mathrm{Ry} = \alpha^2 m_e c^2$. For a real laser, in addition to the field magnitude, importance rests on the laser photon energy normalized by the double Rydberg, 2Ry,

$$\omega_{\mathrm{au}} = \frac{\hbar\omega}{2Ry} \approx \frac{45\mathrm{nm}}{\lambda}, \quad 2Ry = \alpha^2 m_e c^2 \approx 27.2\mathrm{eV}.$$

For the majority of ultra-strong lasers, this parameter is of the order of 10^{-1}: $\omega_{\mathrm{au}} \sim 0.04$ for the Nd-glass laser ($\lambda \approx 1.06$ μm) and $\omega_{\mathrm{au}} \sim 0.06$ for the Ti-sapphire laser ($\lambda \approx 0.8$ μm). Therefore, the following product:

$$\omega_{\mathrm{au}} \left|\frac{d\mathbf{a}}{d\xi}\right|_\alpha = \sqrt{\frac{J}{J_p}}, \quad J_p = \frac{cE_p^2}{4\pi} \approx 2.4 \cdot 10^{25}\mathrm{W/cm}^2, \tag{3}$$

is less than one even for planned intensities (although $|d\mathbf{a}/d\xi|_\alpha$ might be greater than one). Herewith, estimates are made for a 1D wave field, $\mathbf{a} = \mathbf{a}(\xi)$, $\xi = \omega(t - x/c)$, and $0 \leq \xi \leq \xi_{\max}$. Eq. (3) is expressed in terms of the local instantaneous intensity of the laser wave, J. Note that the left hand side (LHS) of Eq. (3) equals the ratio, $|\mathbf{E}|/E_p$, of the wave electric field, $|\mathbf{E}| = \sqrt{4\pi J/c}$, to the characteristic field, $E_p = |e|/\hat{\lambda}_C^2$, constructed from an elementary charge and the Compton wavelength,

$$\hat{\lambda}_C = \frac{\hbar}{m_e c} \approx 3.9 \cdot 10^{-11}\mathrm{cm}, \quad \lambda_C = 2\pi\hat{\lambda}_C \approx 2.4 \cdot 10^{-10}\mathrm{cm}.$$

This field strength is associated with the Coulomb field between the components of a virtual electron-positron *pair* (which are "separated" by the Compton wavelength). Across the interval of intensities bounded by inequality (2) from below and by Eq. (3) from above, that is, at

$$\omega_{\mathrm{au}} \approx \frac{45\mathrm{nm}}{\lambda} \leq \sqrt{\frac{J}{J_p}} \leq 1, \tag{4}$$

the role of important physical effects changes dramatically, incorporating radiation and its back-reaction, and quantum electrodynamic (QED) effects of electron recoil and spin as well as pair production. Given that currently available laser intensities can access this kind of interaction, it is clear that the development of a suitable model is timely.

A. Radiation-dominated laser fields

An accelerated electron in a strong laser field emits high-frequency radiation. The radiation back-reaction decelerates

a)Electronic mail: igorsok@umich.edu.

such an electron, the effect being more pronounced for longer laser pulses.[3] In Ref. 4, a condition for the field to be *radiation-dominated* is formulated in terms of the ratio between the magnitudes of the Lorentz force and the radiation force, which gives

$$\frac{2}{3}\omega_{\mathrm{au}}(\mathcal{E}-p_{\|})_{\alpha}\left(\left|\frac{d\mathbf{a}}{d\xi}\right|_{\alpha}\right)^{2}\geq 1. \tag{5}$$

Herewith, the electron dimensionless energy, $\mathcal{E}$, and its momentum, $\mathbf{p}$, are related to $m_e c^2$ and $m_e c$ correspondingly, and subscript $\|$ herewith denotes the vector projection on the direction of the wave propagation.

While a strong laser pulse interacts with energetic electrons, which move *opposite* the direction of the pulse propagation, the condition $\mathcal{E}-p_{\|}\approx 2\mathcal{E}\gg 1$, facilitates the fulfillment of inequality (5). In the course of a strong laser pulse interacting with a dense plasma, the counterpropagating electrons may be accelerated in a backward direction by a charge separation field. For this reason, the radiation effects in the course of laser-plasma interaction are widely investigated (see Refs. 4–6) and efficient computational tools are in demand.

B. QED-strong laser fields

In QED, an electric field should be treated as strong if it exceeds the Schwinger limit: $|\mathbf{E}|\geq E_S=m_e c^2/(|e|\hat{\lambda}_C)$ (see Ref. 7). Such field is potentially capable of separating a virtual electron-positron pair providing an energy, which exceeds the electron rest mass energy, $m_e c^2$, to a charge, $e=\mp|e|$, over an acceleration length as small as the Compton wavelength. Typical effects in QED-strong fields are high-energy photon emission from electrons or positrons and electron-positron pair creation from high-energy photons (see Refs. 8–10).

Here, we assume that the field invariants (see Ref. 11) are small as compared to the Schwinger field

$$|E^2-B^2|\ll E_S^2,\qquad |(\mathbf{E}\cdot\mathbf{B})|\ll E_S^2, \tag{6}$$

where $\mathbf{B}$ is the magnetic field. Below, the term "QED-strong field" is only applied to the field experienced by a particle. For example, a particle in the 1D wave field may experience a QED-strong field, $E_0=|d\mathbf{A}/d\xi|\omega(\mathcal{E}-p_{\|})/c$, because the laser frequency is Doppler upshifted in the comoving frame of reference. The Lorentz-transformed field exceeds the Schwinger limit, if

$$\chi=\frac{2}{3}E_0/E_S=\frac{2\hat{\lambda}_C}{3\hat{\lambda}}(\mathcal{E}-p_{\|})\left|\frac{d\mathbf{a}}{d\xi}\right|\gg 1, \tag{7}$$

where $\hat{\lambda}=c/\omega$. Numerically, the parameter, χ, equals

$$\chi=\frac{3}{2}\omega_{\mathrm{au}}(\mathcal{E}-p_{\|})_{\alpha}\left|\frac{d\mathbf{a}}{d\xi}\right|_{\alpha}\approx 0.7\frac{(\mathcal{E}-p_{\|})}{10^3}\sqrt{\frac{J}{10^{23}[\mathrm{W/cm^2}]}}.$$

C. Estimates for laser-driven electrons

In the critical parameters as in inequalities (5) and (7), the factor, $\mathcal{E}-p_{\|}$ is not linked to the wave intensity in the case where electrons are accelerated by an external source. In the course of the laser-plasma interaction, however, for bulk electrons $(\mathcal{E}-p_{\|})\sim\mathcal{E}\sim|\mathbf{p}_{\perp}|$. As long as the radiation back-reaction does not dominate, the conservation law for the generalized momentum of an electron gives $\mathbf{p}_{\perp}\approx-\mathbf{a}$, and the LHS of inequality (5) may be evaluated in terms of the laser intensity. The wave becomes radiation-dominated, if

$$J\geq J_p(\omega_{\mathrm{au}})^{4/3}\sim(3-5)\cdot 10^{23}\mathrm{W/cm^2}.$$

Less certain is the estimate for the significance of QED effects. On one hand, for fields just approaching the radiation-dominated regime, QED effects are already not fairly neglected, $\chi\sim(3/2)(\omega_{\mathrm{au}})^{1/3}\approx(0.5-0.6)$. On the other hand, in radiation-dominated fields, the estimate for $\mathcal{E}$ that we used above is not reliable. Because of this complexity, we surmise that the significance of QED effects in this regime can only be verified by direct numerical simulations.

D. Paper content and structure

Numerical simulations of laser-plasma interactions become increasingly complicated while proceeding to higher intensities. At intensities $J\geq 2\cdot 10^{22}$ W/cm^2, the model should incorporate the radiation back-reaction on the emitting electron. In this range, $\chi\ll 1$ for bulk electrons, making QED-effects negligible. This model is presented in Sec. II. At $J\geq 3\cdot 10^{23}$ W/cm^2, QED corrections should be incorporated to achieve quantitative accuracy for electrons with $\chi\sim 1$. These corrections may be found in Sec. III. At larger intensities, $J\geq 10^{24}$ W/cm^2, the high-energy photons emitted by electrons and positrons produce a macroscopically large number of electron-positron pairs, as shown in Sec. IV.

In each section, we first summarize the theoretical model. Then we provide an analytical solution which may be used to benchmark numerical models. After this, we describe the elements of the numerical scheme.

II. QED-WEAK FIELDS ($\chi\ll 1$)

A. Theoretical notes

1. Emission spectrum

In Ref. 12, the spectral and angular distribution, $d\mathcal{E}_{\mathrm{rad}}/(d\omega' d\mathbf{n})$, of the radiation energy, emitted by an electron with position, $\mathbf{x}(t)$, and velocity, $\mathbf{v}(t)$, and related to the interval of frequency, $d\omega'$, and to the element of solid angle, $d\mathbf{n}$, for a polarization vector, $\mathbf{l}$, is described with the following formula:

$$\frac{d\mathcal{E}_{\mathrm{rad}}(\omega',\mathbf{n},\mathbf{l})}{d\omega' d\mathbf{n}}=\frac{(\omega')^2}{4\pi^2 c}|(\mathbf{A}_{\mathrm{cl}}(\omega')\cdot\mathbf{l}^*)|^2. \tag{8}$$

Here, the vector amplitude of emission, $\mathbf{A}_{\mathrm{cl}}(\omega')$, is given by the following equation:

$$\mathbf{A}_{\mathrm{cl}}(\omega',\mathbf{n})=\frac{e}{c}\int_{-\infty}^{+\infty}\mathbf{v}(t)\exp\left(i\omega'\left\{t-\frac{[\mathbf{n}\cdot\mathbf{x}(t)]}{c}\right\}\right)dt,$$

see Eq. (14.67) in Ref. 12. We express $d\mathcal{E}_{\mathrm{rad}}/(d\omega' d\mathbf{n})$ in terms of the time integral of the radiation loss rate, $dI_{\mathrm{cl}}/(d\omega' d\mathbf{n})$,

which is related to the unit of time, the element of a solid angle, and the frequency interval, and is summed over polarizations,

$$\frac{\partial}{\partial t}\left[\sum_{\mathbf{l}}\frac{d\mathcal{E}_{\rm rad}}{d\omega' d\mathbf{n}}\right]=\frac{dI_{\rm cl}(t)}{d\omega' d\mathbf{n}}.$$

The spectral and angular distribution of the radiation loss rate is given by the Fourier integral,

$$\frac{dI_{\rm cl}(\tau)}{d\omega' d\mathbf{n}}=-\frac{e^2(\omega')^2}{4\pi^2 c\mathcal{E}(\tau)}\int_{-\infty}^{+\infty}\left[p\left(\tau+\frac{\zeta}{2}\right)\cdot p\left(\tau-\frac{\zeta}{2}\right)\right]\times\exp\left\{ic\int_{\tau-\zeta/2}^{\tau+\zeta/2}[k'\cdot p(\tau')]d\tau'\right\}d\zeta.$$

The cogent feature of the particle relativistic motion in strong laser fields is that the emitted radiation is abruptly beamed about the direction of the velocity vector, $\mathbf{p}(\tau)/|\mathbf{p}(\tau)|$. Therefore, the angular spectrum of emission can be approximated with the Dirac function,

$$\frac{dI_{\rm cl}(\tau)}{d\omega' d\mathbf{n}}=\delta^2\left(\mathbf{n}-\frac{\mathbf{p}}{|\mathbf{p}|}\right)\frac{dI_{\rm cl}(\tau)}{d\omega'}.$$

In the frequency spectrum of emission,

$$\frac{dI_{\rm cl}(\tau)}{d\omega'}=\frac{e^2\omega'}{2\pi c\mathcal{E}^2(\tau)}\int_{-\infty}^{+\infty}\frac{1}{\zeta}\left[p\left(\tau+\frac{\zeta}{2}\right)\cdot p\left(\tau-\frac{\zeta}{2}\right)\right]\times\sin\left[\frac{\omega'}{\mathcal{E}(\tau)}\left(\frac{\zeta}{2}+\int_{\tau-\zeta/2}^{\tau+\zeta/2}\{[p(\tau)\cdot p(\tau')]-1\}d\tau'\right)\right]d\zeta,$$

for relativistically strong wave field, satisfying Eq. (1), the sine function varies rapidly, so that the main contribution to the integral determining the emission spectrum comes from a brief time interval with small values of ζ, resulting in a *universal* emission spectrum,

$$\frac{dI_{\rm cl}(\tau)}{d\omega'}=I_{\rm cl}\frac{Q_{\rm cl}(r)}{\omega_c},\quad I_{\rm cl}=-\frac{2e^2(f_{Le}\cdot f_{Le})}{3m_e^2c^3},\tag{9}$$

$$Q_{\rm cl}(r)=\frac{9\sqrt{3}}{8\pi}r\int_r^\infty K_{5/3}(r')dr',\quad r=\frac{\omega'}{\omega_c},\tag{10}$$

$$\omega_c=\mathcal{E}\chi.\tag{11}$$

Here, $Q_{\rm cl}(r)$ is the unity-normalized spectrum of the gyrosynchrotron emission, such that $\int Q_{\rm cl}(r)dr=1$ and $K_\nu(r)$ are MacDonald functions. We use the dimensionless photon frequency, $\tilde{\omega}'=\hbar\omega'/(m_ec^2)$, the characteristic frequency, $\tilde{\omega}_c=\hbar\omega_c/(m_ec^2)$, and the dimensionless wave vector, $\tilde{\mathbf{k}}'=\hbar\mathbf{k}'$, for emitted γ-photons and omit tildes in the formulae. Both the radiation energy loss rate, $I_{\rm cl}$, and the QED-strength parameter,

$$\chi=\frac{3}{2}\frac{\hat{\lambda}_C\sqrt{-(f_{Le}\cdot f_{Le})}}{m_ec^2},\tag{12}$$

are expressed in terms of the 4-square of the Lorentz 4-force: $f^\mu_{Le}=\mathcal{E}(\mathbf{f}_{Le}\cdot\mathbf{u}/c,\mathbf{f}_{Le})$, where $\mathbf{u}=c\mathbf{p}/\sqrt{1+\mathbf{p}^2}$ is the velocity and $\mathbf{f}_{Le}=e\mathbf{E}+\frac{e}{c}[\mathbf{u}\times\mathbf{B}]$ is the Lorentz three-force.

Thus, the acceleration of electrons by a laser pulse (or by a wake-field, which may also cause the relativistic quivering motion of electrons) must be accompanied by gyrosynchrotron-like emission spectrum (which is actually observed—see Refs. 13 and 14). The general character of such emission spectrum had been noted in Ref. 13 (this comment may be also found in Sec. 77 in Ref. 11). The material of the present subsection was published in Ref. 15.

2. Equation for the radiation emission and transport

The above considerations justify the method for calculating the high frequency emission as described in Ref. 3 (see also Ref. 13). In addition to calculating the electromagnetic fields on the grid using a particle-in-cell (PIC) scheme, one can also account for the higher-frequency (subgrid) emission, by calculating its instantaneously radiated spectrum. Compared with direct calculation of the right hand side (RHS) of Eq. (8) (the means of calculating the emission used, for example, in Refs. 16 and 17), the approach suggested here, though mathematically equivalent, may be decidedly more efficient.

Generally, the radiation transport equation (RTE, cf. Ref. 18) should be solved for the radiation energy density, related to the element of volume, dV (herewith, the symbol $\sum_{\mathbf{l}}$ is omitted),

$$\mathcal{I}=\frac{d\mathcal{E}_{\rm rad}}{d\omega' d\mathbf{n}dV}.$$

An electron located at the point, $\mathbf{x}=\mathbf{x}_e(t)$, contributes to the RHS of the RTE as follows:

$$\frac{\partial\mathcal{I}}{\partial t}+c(\mathbf{n}\cdot\nabla)\mathcal{I}=\sum_e\frac{I_{\rm cl}Q_{\rm cl}(r)}{\omega_c}\delta^2\left(\mathbf{n}-\frac{\mathbf{p}}{p}\right)\delta^3(\mathbf{x}-\mathbf{x}_e).$$

The LHS of the RTE describes the radiation transport, while in the RHS, in addition to the emission source, there should be the terms accounting for the radiation absorption and scattering. However, at $\chi\ll1$ and at realistic plasma densities, these effects may be neglected. Under these circumstances, the RTE can be easily integrated over time and space, giving

$$\frac{d\mathcal{E}_{\rm rad}}{d\omega' d\mathbf{n}}=\int_0^t\left(\sum_e\frac{I_{\rm cl}Q_{\rm cl}(r)}{\omega_c}\delta^2(\mathbf{n}-\frac{\mathbf{p}}{p})\right)dt.\tag{13}$$

Since Eq. (13) depends on frequency only via $Q_{\rm cl}(r)$, one can calculate instead of Eq. (13) an integral as follows:

$$\frac{d\mathcal{E}^{(m)}_{\rm rad}}{d\mathbf{n}d\bar{\omega}}=\int_0^t\left[\sum_e\frac{I_{\rm cl}}{\omega_c}\delta^2\left(\mathbf{n}-\frac{\mathbf{p}}{p}\right)\delta(\log\bar{\omega}-\log\omega_c)\right]dt.$$

Once this modified spectrum has been integrated over the whole simulation time, a true spectral distribution can be recovered using a simple convolution as follows:

$$\frac{d\mathcal{E}_{\rm rad}(\omega',\mathbf{n})}{d\mathbf{n}d\omega'}=\int Q_{\rm cl}\left(\frac{\omega'}{\bar{\omega}}\right)\frac{d\mathcal{E}^{(m)}_{\rm rad}(\bar{\omega},\mathbf{n})}{d\mathbf{n}d\bar{\omega}}d\log\bar{\omega}.\tag{14}$$

Manifestly, the result is the same, which allows one to avoid calculating the spectrum, $Q_{\rm cl}(r)$, at each time step.

3. Equation for electron motion: Accounting the radiation back-reaction

Here, we use the equation of motion for a radiating electron as derived in Refs. 3 and 19. In 4-vector form, this equation may be written for the electron 4-momentum, p^α, normalized per $m_e c$, in terms of the Lorentz 4-force $f^\alpha_{Le} = eF^{\alpha\beta}p_\beta$ and the field 4-tensor $F^{\alpha\beta} = (\mathbf{E}, \mathbf{B})$,

$$\frac{dp^\alpha}{d\tau} = \frac{e}{m_e c^2} F^{\alpha\beta}\frac{dx_\beta}{d\tau} - \frac{I_{\rm cl}p^\alpha}{mc^2}, \tag{15}$$

$$\frac{dx^\alpha}{d\tau} = cp^\alpha + \frac{\tau_0 f^\alpha_{Le}}{m_e}, \quad \tau_0 = \frac{2e^2}{3m_e c^3}. \tag{16}$$

Three-vector formulation of Eqs. (15) and (16) is

$$\frac{d\mathbf{p}}{dt} = \frac{\mathbf{f}_{Le}}{m_e c} + \frac{e[\bar{\mathbf{u}}\times\mathbf{B}]}{m_e c^2} - \frac{\mathbf{u}\mathcal{E}^2(\bar{\mathbf{u}}\cdot\mathbf{f}_{Le})}{m_e c^3}, \tag{17}$$

$$\frac{d\mathbf{x}}{dt} = \mathbf{u} + \bar{\mathbf{u}}, \quad \bar{\mathbf{u}} = \frac{\tau_0}{m_e}\frac{\mathbf{f}_{Le} - \mathbf{u}(\mathbf{u}\cdot\mathbf{f}_{Le})/c^2}{1 + \tau_0(\mathbf{u}\cdot\mathbf{f}_{Le})/(mc^2)},$$

$\bar{\mathbf{u}}$ being the back-reaction effect on the electron velocity.

4. Comparison with the Landau-Lifshitz (LL) equation

Many authors simulate the motion of an emitting electron using the equation suggested by LL (see Eq. (76.3) in Ref. 11), motivating a comparison with the approach we use. To simplify the formulae, we introduce the 4-velocity, u^i, and normalize the field tensor,

$$u^\alpha = \frac{1}{c}\frac{dx^\alpha}{d\tau}, \quad \tilde{F}^{\alpha\beta} = \frac{\tau_0 eF^{ik}}{m_e c} = \frac{2\alpha F^{ik}}{3E_S}.$$

All 4-vector equations in this paragraph are written without indices, and the tensor multiplication is denoted with dot-product and/or powers of tensor, e.g., $\tilde{F}\cdot u = \tilde{F}^{ik}u_k$, $\tilde{F}^2\cdot u = \tilde{F}\cdot\tilde{F}\cdot u = \tilde{F}^{ik}\tilde{F}_{kl}u^l$, etc. Now we re-write the LL equation

$$\frac{du}{d\tau} = \frac{1}{\tau_0}\tilde{F}\cdot\left(u + \tilde{F}\cdot u\right) + \frac{d\tilde{F}}{d\tau}\cdot u - \frac{u}{\tau_0}(u\cdot\tilde{F}^2\cdot u) \tag{18}$$

and compare it with Eqs. (15) and (16),

$$\frac{dp}{d\tau} = \frac{1}{\tau_0}\tilde{F}u - \frac{p}{\tau_0}(p\cdot\tilde{F}^2\cdot p), \quad u = p + \tilde{F}\cdot p. \tag{19}$$

Solving the momentum from the second of Eqs. (19), $p = \sum_{n=0}^{\infty}(-\tilde{F})^n\cdot u$. Accounting for the anti-symmetry of the field tensor, the first of Eqs. (19) may be re-written for 4-velocity and 4-acceleration, similarly to Eq. (18),

$$\frac{du}{d\tau} = \frac{1}{\tau_0}\tilde{F}\cdot\left(u + \tilde{F}\cdot u\right) + \frac{d\tilde{F}}{d\tau}\cdot\sum_{n=0}^{\infty}(-\tilde{F})^n\cdot u - \frac{u}{\tau_0}(u\cdot\sum_{n=1}^{\infty}\tilde{F}^{2n}\cdot u). \tag{20}$$

The only distinction from Eq. (18) is that in Eq. (20), the infinite series are present, while in Eq. (18), there are only starting terms of these series.

How large is the difference *numerically*? For the second series, one may evaluate both the total sum,

$$u\cdot\sum_{n=1}^{\infty}\tilde{F}^{2n}\cdot u = p\cdot\tilde{F}^2\cdot p = \left(\frac{2}{3}\alpha\right)^2\left(\frac{4}{9}\chi^2\right),$$

and the residual sum, omitted in Eq. (18),

$$u\cdot\sum_{n=2}^{\infty}\tilde{F}^{2n}\cdot u = \left(\frac{2}{3}\alpha\right)^4\left(\frac{4}{9}\chi^2\frac{E^2 - B^2}{E_s^2} + \frac{(\mathbf{E}\cdot\mathbf{B})^2}{E_s^4}\right).$$

The residual sum is reduced by a factor, $(2\alpha/3)^2\cdot(E^2 - B^2)/E_S^2$, which is small according to inequality (6).

How *theoretically* important is the distinction between the two approaches? We discussed this issue in Refs. 3 and 19 and noted that the LL equation conserves neither the generalized momentum of electron nor the total energy-momentum of the system consisting of an emitting electron, the external field, and the radiation. Another distinction is that the LL approach maintains the identity, $u^2 = 1$, while Eqs. (19) maintain more important identity, $p^2 = 1$, turning to the Dirac equation in the limit of QED-strong fields. For the square of the 4-velocity, we obtain

$$u^2 = p^2 - p\cdot\tilde{F}^2\cdot p \approx 1 - 1.05\cdot 10^{-5}\chi^2, \tag{21}$$

which is not exactly unity, but in QED-weak fields, $\chi \ll 1$, the distinction is negligible.

The *computational* advantages of Eqs. (19) as compared to the LL equation are first, the higher efficiency: compare the compact expression for three-force in Eq. (17) with that given in Ref. 11 (see Sec. 77, problem 2); and second, the numerical scheme for Eq. (17) is more reliable, as it is bound to yield total energy conservation. Thus, even for fields in the QED weak regime, the use of Eqs. (19) is more suitable than the use of the LL equation.

B. Analytical solution

Pertaining to the validation against a semi-analytical theory, we begin by describing the spectrum of emission from an electron in the field of a 1D circularly polarized wave. A constant wave amplitude, a_0 is assumed to be *below* the radiation-dominated regime. In this case, $\mathbf{p}_\perp \approx -\mathbf{a}$, so that $\mathcal{E}^2 - {p_\parallel}^2 = 1 + a_0^2$. The *modified* spectrum can be expressed in terms of the characteristic frequency, which is a function of the current value of the electron energy,

$$\frac{\omega_c}{\omega_{c0}} = 1 + \frac{(\mathcal{E} - p_\parallel)^2}{1 + a_0^2}, \tag{22}$$

as well as the parameter, ω_{c0}, which is introduced as the following function of the wave amplitude and frequency,

$$\omega_{c0} = \frac{3}{4}\omega_{\rm au}\alpha^2\left(a_0 + a_0^3\right). \tag{23}$$

The maximum frequency of emission is determined by the initial momentum of electron,

$$\frac{\omega_{c\max}}{\omega_{c0}} = 1 + \frac{(\mathcal{E} - p_{||})^2_{\xi=0}}{1 + a_0^2}.$$

Then, $\xi^*(\xi)$ is a normalized phase,

$$\xi^* = \left(\frac{2}{3}\alpha^3 \omega_{\rm au} a_0^2 \sqrt{1 + a_0^2}\right)\xi. \tag{24}$$

For the whole pulse, the total normalized phase,

$$\xi^*_\infty = \frac{2}{3}\alpha^3 \omega_{\rm au} a_0^2 \sqrt{1 + a_0^2}\xi_{\max} \approx \frac{2}{3}\left(\frac{J}{J_p}\right)^{3/2} \frac{\xi_{\max}}{(\omega_{\rm au})^2},$$

characterizes the capability of the pulse to arrest the counter-propagating electron by means of the radiation back-reaction. Particularly, a pulse of duration corresponding to $\xi^*_\infty \geq 1$ arrests an electron of any energy. The modified spectrum has a shape close to a power-law (see derivation details in Ref. 20),

$$\frac{d\mathcal{E}^{(m)}_{\rm rad}}{d\bar{\omega}} = \frac{m_e c^2 \sqrt{1 + \mathbf{a}^2}}{4\omega_{c0}} \frac{\bar{\omega}/\omega_{c0}}{(\bar{\omega}/\omega_{c0} - 1)^{3/2}}, \tag{25}$$

$$\frac{\omega_{c\min}}{\omega_{c0}} \leq \frac{\bar{\omega}}{\omega_{c0}} \leq \frac{\omega_{c\max}}{\omega_{c0}}, \tag{26}$$

where $\omega_{c\min}$ should be found from Eq. (22), for given ξ^*_∞,

$$\frac{\omega_{c\min}}{\omega_{c0}} = 1 + \left(\frac{1}{\sqrt{\omega_{c\max}/\omega_{c0} - 1}} + \xi^*_\infty\right)^{-2}. \tag{27}$$

The true (transformed) spectrum can be obtained from the modified spectrum as in Eq. (25) by applying a convolution transformation following Eq. (14). The longer the pulse, the more softened and broadened the radiation spectrum becomes (see Fig. 1).

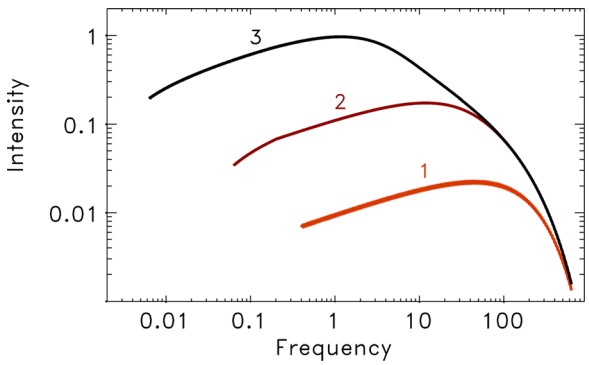

FIG. 1. (Color online) The shape of normalized spectra, $(d\mathcal{E}_{\rm rad}/d\omega')\cdot[4\omega_{c0}/(m_e c^2\sqrt{1+\mathbf{a}^2})]$, versus the normalized frequency, ω'/ω_{c0}, for different pulse duration. The figure is scalable, particular choice of physical parameters, may be the following: $|\mathbf{a}| = 50$, $\mathcal{E} = 180$ MeV, pulse durations are 5 fs (curve 1), 36 fs (curve 2), and 220 fs (curve 3). The spectrum broadening and softening is due to the radiation reaction. In the absence of this reaction, curve 1 without changing its shape would scale proportionally to the pulse duration. A zero value of $\log(\omega'/\omega_{c0})$ corresponds to ≈ 150 keV.

C. Numerical model

Now we introduce the following normalized variables:

$$\tilde{t} = \omega t, \qquad \tilde{\mathbf{x}} = \omega \mathbf{x}/c, \qquad \tilde{\mathbf{u}} = \frac{\mathbf{u}}{c},$$
$$\tilde{\mathbf{E}} = \frac{|e|\mathbf{E}}{m_e c\omega}, \qquad \tilde{\mathbf{B}} = \frac{|e|\mathbf{B}}{m_e c\omega}, \qquad \tilde{\mathbf{j}} = \frac{4\pi|e|\mathbf{j}}{m_e c\omega^2}.$$

Note that the electric current density, $\tilde{\mathbf{j}}$, is normalized per $|e|n_{\rm cr}c$, where $n_{\rm cr} = m_e\omega^2/(4\pi e^2)$ is the critical density. Below, we use these dimensionless variables and omit tildes in notations. The equations of motion for electrons and positrons read

$$\frac{d\mathbf{p}_{e,p}}{dt} = \mathbf{f}_{Le,p} \mp [\bar{\mathbf{u}}_{e,p} \times \mathbf{B}] - \mathbf{u}_{e,p}\mathcal{E}^2_{e,p}(\mathbf{f}_{Le,p} \cdot \bar{\mathbf{u}}_{e,p}),$$
$$\frac{d\mathbf{x}_{e,p}}{dt} = \mathbf{u}_{e,p} + \bar{\mathbf{u}}_{e,p}, \quad \mathcal{E}_{e,p} = \sqrt{1 + \mathbf{p}^2_{e,p}}, \quad \mathbf{u}_{e,p} = \frac{\mathbf{p}_{e,p}}{\mathcal{E}_{e,p}},$$

the normalized Lorentz force and $\bar{\mathbf{u}}$ being

$$\mathbf{f}_{Le,p} = \mp(\mathbf{E} + [\mathbf{u}_{e,p} \times \mathbf{B}]), \quad \varepsilon = \tau_0\omega = \frac{2}{3}\alpha^3\omega_{\rm au}$$
$$\bar{\mathbf{u}}_{e,p} = \varepsilon\frac{\mathbf{f}_{Le,p} - \mathbf{u}_{e,p}(\mathbf{u}_{e,p} \cdot \mathbf{f}_{Le,p})}{1 + \varepsilon(\mathbf{u}_{e,p} \cdot \mathbf{f}_{Le,p})}. \tag{28}$$

For reference, we also provide the energy equation

$$\frac{d\mathcal{E}_{e,p}}{dt} = \mp([\mathbf{u}_{e,p} + \bar{\mathbf{u}}_{e,p}] \cdot \mathbf{E}) - \mathcal{E}^2_{e,p}(\mathbf{f}_{Le,p} \cdot \bar{\mathbf{u}}_{e,p}). \tag{29}$$

For ions with the charge number, Z, and the mass, M_i, the momentum is normalized per $M_i c$, so that, in their equation of motion, the electron-to-ion mass ratio comes

$$\frac{d\mathbf{p}_i}{dt} = \frac{Z}{M_i/m_e}(\mathbf{E} + [\mathbf{u}_i \times \mathbf{B}]), \tag{30}$$

$$\frac{d\mathbf{x}_i}{dt} = \mathbf{u}_i, \quad \mathbf{u}_i = \frac{\mathbf{p}_i}{\sqrt{1 + \mathbf{p}_i^2}}. \tag{31}$$

Below we assume that $Z = 1$ and $M_i = M_p$ is the proton mass. The normalized Maxwell equations read

$$\frac{\partial\mathbf{E}}{\partial t} + \mathbf{j} = \nabla \times \mathbf{B}, \qquad \frac{\partial\mathbf{B}}{\partial t} = -\nabla \times \mathbf{E}. \tag{32}$$

1. Macroparticles and their current

We assume that a rectangular grid splits the computational domain into the control volumes (cells), $\Delta V = \prod \Delta x_k$. If the electron density equals $n_{\rm cr}$, there are $n_{\rm cr}\Delta V$ electrons per cell. The latter number is typically very large, so that the plasma electrons cannot be simulated individually and they are combined into macroparticles with a large number of "electrons-per-particle," N_{epp}. In a plasma of critical density, the number of (macro) particles per cell is $N_{ppc} = n_{\rm cr}\Delta V/N_{epp}$.

The electron current density inside the given cell is expressed in terms of the sum over electron macroparticles in this cell. As long as the electric current density is

normalized per $n_{\rm cr}c$, the contribution to the latter sum from each macroparticle equals $-(1/N_{ppc})d\mathbf{x}_e/dt$. On adding the contributions from positrons and protons, we obtain

$$\mathbf{j} = \frac{-\sum_e (\mathbf{u}_e + \bar{\mathbf{u}}_e) + \sum_p (\mathbf{u}_p + \bar{\mathbf{u}}_p) + \sum_i \mathbf{u}_i}{N_{ppc}}. \quad (33)$$

2. Energy integral and energy balance

We now establish the relationship between the energy integral and the finite sum, which represents this integral in simulations. Particularly, the field energy may be calculated as the total of point-wise field magnitudes squared: $\mathcal{E}_{\rm field} = \frac{1}{2}\sum_{cells}(\mathbf{E}^2 + \mathbf{B}^2)$, which is by a factor of $\mathcal{E}_0 = m_e c^2 (n_{\rm cr}\Delta V)$ different from the dimensional field energy. Now consider the total plasma energy, which includes the particle energy as well,

$$\mathcal{E}_{\rm plasma} = \mathcal{E}_{\rm field} + \frac{\sum_{cells}\left(\frac{M_i}{m_e}\sum_i \mathcal{E}_i + \sum_e \mathcal{E}_e + \sum_p \mathcal{E}_p\right)}{N_{ppc}}.$$

Equations (29), (32), and (33) give $d(\mathcal{E}_{\rm plasma} + \mathcal{E}_{\rm rad})/dt = 0$, where

$$\frac{d\mathcal{E}_{\rm rad}}{dt} = \frac{\sum_{cells}\sum_{e,p}\mathcal{E}_{e,p}^2(\mathbf{f}_{Le,p}\cdot\bar{\mathbf{u}}_{e,p})}{N_{ppc}} \quad (34)$$

is the radiation energy loss rate. Therefore, the contribution from electrons and positrons to the dimensionless radiation energy at each time step, Δt, is calculated as $\mathcal{E}_{e,p}^2(\mathbf{f}_{Le,p}\cdot\bar{\mathbf{u}}_{e,p})\Delta t/N_{ppc}$. Once integrated over the simulation time, the radiation energy may be converted to physical units on multplying it by a factor of $\mathcal{E}_0$.

3. Algorithmic implementation

The algorithmic changes to the standard PIC scheme are minimal as long as we ignore the radiation transport and only integrate over time the energy emitted by electrons (and positrons, if any). To collect the radiation, we introduce energy bins (an array) $\mathcal{E}_{{\rm rad}\,ijk}(\log(\bar{\omega})_i, \theta_j, \varphi_k)$, which discretize the *modified* frequency-angular spectrum of emission. Inside the desired interval of the photon energies, we introduce a logarithmic grid, $\log(\bar{\omega})_i$, equally spaced with a step, $\Delta\log(\bar{\omega})$. We also introduce a grid, θ_j, φ_k, for the two polar angles of the spherical coordinate system, with $\Delta\mathbf{n}_{jk}$ being the element of solid angle, $\Delta\mathbf{n}_{jk} = \sin(\theta_j)\Delta\theta\Delta\varphi$.

To calculate both the spectrum of emission and the radiation back-reaction, we modify only that part of the PIC algorithm which accounts for the electron motion. Specifically, we employ the standard leapfrog numerical scheme which involves, among others, the following stages: (1) for each electron macroparticle, update momentum through the time step by adding the Lorentz force, following the Boris scheme: $\mathbf{p}_e^{n+1/2} = \mathbf{p}_e^{n-1/2} + \Delta t\,\mathbf{f}_{Le}(\mathbf{E}^n, \mathbf{B}^n)$; (2) solve the energy and the velocity from the updated momentum: $\mathcal{E}_e^{n+1/2} = \sqrt{1 + (\mathbf{p}_e^{n+1/2})^2}$, $\mathbf{u}_e^{n+1/2} = \mathbf{p}_e^{n+1/2}/\mathcal{E}_e^{n+1/2}$; (3) use the calculated velocity to update the particle coordinates: $\mathbf{x}_e^{n+1} = \mathbf{x}_e^n + \mathbf{u}_e^{n+1/2}\Delta t$ and account for the contribution of the electric current element to the Maxwell equations. Again, these stages are standard and may be found in Ref. 21. We introduced new steps into this algorithm between stages (2) and (3) as follows.

2.1. Once stage (2) is done, recover the Lorentz force: $\mathbf{f}_{Le} = (\mathbf{p}_e^{n+1/2} - \mathbf{p}_e^{n-1/2})/\Delta t$.
2.2. Find $\chi = \frac{3}{2}\omega_{\rm au}\alpha^2\mathcal{E}_e^{n+1/2}\sqrt{\mathbf{f}_{Le}^2 - (\mathbf{f}_{Le}\cdot\mathbf{u}_e^{n+1/2})^2}$.
2.3. Find $\bar{\mathbf{u}}_e$ by putting $\mathbf{f}_{Le}$ and $\mathbf{u}_e^{n+1/2}$ into Eq. (28).
2.4. Calculate $\omega_c = \mathcal{E}_e^{n+1/2}\chi$ and find the discrete value of $\log(\bar{\omega})_i$ most close to $\log\omega_c$. Find the angles, θ_j, φ_k closest to the direction of $\mathbf{p}_e^{n+1/2}$. Add the radiation energy into the proper bin

$$\mathcal{E}_{{\rm rad}\,ijk} \to \mathcal{E}_{{\rm rad}\,ijk} + \frac{(\mathcal{E}_e^{n+1/2})^2(\mathbf{f}_{Le}\cdot\bar{\mathbf{u}}_e)\Delta t}{\omega_c N_{ppc}\Delta\log(\bar{\omega})\Delta\mathbf{n}_{jk}}.$$

2.5. Add the radiation force: $\mathbf{p}_e^{n+1/2} \to \mathbf{p}_e^{n+1/2} + \Delta t\{-[\bar{\mathbf{u}}_e \times \mathbf{B}^n] - \mathbf{u}_e^{n+1/2}(\mathcal{E}_e^{n+1/2})^2(\mathbf{f}_{Le}\cdot\bar{\mathbf{u}}_e)\}$.
2.6. Find $\mathbf{u}_e^{n+1/2} = \mathbf{p}_e^{n+1/2}/\sqrt{1 + (\mathbf{p}_e^{n+1/2})^2} + \bar{\mathbf{u}}_e$ and use this velocity through stage (3).

Note that the algorithm modification is applied only to electrons (positrons), keeping unchanged the ion motion as well as the fields.

The frequency-angular spectrum may be reduced to a frequency one: $\mathcal{E}_{{\rm rad}\,i} = \sum_{jk}\mathcal{E}_{{\rm rad}\,ijk}\Delta\mathbf{n}_{jk}$, to an angular one: $\mathcal{E}_{{\rm rad}\,jk} = \sum_i \mathcal{E}_{{\rm rad}\,ijk}\bar{\omega}_i\Delta\log(\bar{\omega})$ or to the total radiation energy: $\mathcal{E}_{\rm rad} = \sum_{ijk}\mathcal{E}_{{\rm rad}\,ijk}\bar{\omega}_i\Delta\log(\bar{\omega})\Delta\mathbf{n}_{jk}$.

While postprocessing the results, we apply the convolution transformation, Eq. (14), to the radiation spectrum and multiply it by $\mathcal{E}_0$. The resulting spectrum, $d\mathcal{E}_{\rm rad}/(d\mathbf{n}d\omega')$, is a function of $\log[\hbar\omega'/(m_e c^2)]$.

D. Simulation result

The analytical solution presented in Sec. II B has been used to benchmark the numerical scheme. In the test simulation, electrons with an initial momentum, $p_\parallel = 300$, propagate toward the laser pulse with sharp (2λ) fronts. The circularly polarized laser pulse has amplitude, $|\mathbf{a}| = 15$, and duration, $100(2\pi/\omega)$. Interacting with the pulse, the particles radiate energy, finally approaching momentum of $p_\parallel \approx 130$.

In Fig. 2(a), the spectrum of the resulting radiation $d\mathcal{E}_{\rm rad}/d\omega'$ is shown. We also provide the modified spectrum (the distribution over $\bar{\omega} = \omega_c$), which is close to satisfying a power law, and in full agreement with the analytical solution. In Figs. 2(b) and 2(c), evolution typical of the angular radiation distribution, $d\mathcal{E}_{\rm rad}/d\mathbf{n}$, is provided for the same simulation. One can see that the majority of the radiation is concentrated in a narrow angle with respect to the direction of backscattered light (0°). A softer part of the radiation exhibits a wider angular distribution and becomes less intense [Fig. 2(c)].

III. QED-MODERATE FIELDS ($\chi \sim 1$)

When χ is not small ($J \sim 3\cdot 10^{23}$ W/cm^2), QED effects come into play. Here, we describe how to *extend* the methods

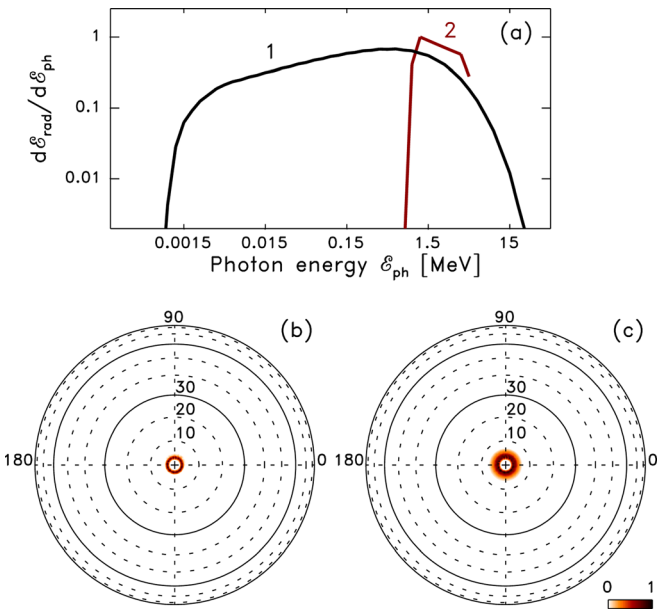

FIG. 2. (Color online) Test simulation result: (a) radiation energy spectrum (line 1), $d\mathcal{E}_{\rm rad}/d\omega'$, and the modified spectrum, $d\mathcal{E}_{\rm rad}/d\bar{\omega}$ (line 2); (b) and (c) the angular distribution of the radiation at instants: (b) t = 10 T, (c) t = 50 T, where $T = 2\pi/\omega$.

used above towards finite χ. This is achieved by applying realistic QED emission spectra as derived in Ref. 15, with the radiation force modified accordingly.

This approach is applicable as long as we ignore the onset of some *new* effects which are only pertinent to QED-strong fields. Specifically, while employing the radiation force, $dp^{\mu}_{\rm rad}/d\tau$, it is admitted that the change in the electron momentum, $d\tau \cdot dp^{\mu}_{\rm rad}/d\tau$, within the infinitesimal time interval, $d\tau$, is also infinitesimal. This "Newton's law" approximation is pertinent to classical physics, and it ignores the point that the change in the electron momentum at $\chi \sim 1$ is essentially finite because of the finite momentum of emitted photon. The approximation, however, is highly efficient and allows one to avoid time-consuming statistical simulations. Its error tends to zero as $\chi \to 0$, and it is sufficiently small at $\chi \sim 1$.

Another effect which we ignore in this section is pair production due to γ-photon absorption in the strong laser field. This neglect allows us to avoid solving the computationally intense radiation transport problem.

A. Theoretical notes

1. Emission spectrum

The emission probability found in Ref. 15 within the framework of QED can be reformulated in a form similar to Eq. (8). The polarized part of emission may be reduced to Eq. (8) with the modified vector amplitude,

$$\mathbf{A}_{\rm QED}(\omega') = \sqrt{\frac{1}{C_{fi}}}\mathbf{A}_{\rm cl}\left(\frac{\omega'}{C_{fi}}\right), \quad C_{fi} = \frac{(k\cdot p_i)}{(k\cdot p_f)},$$

where subscript i and f denote the parameters of an electron prior to and after the emission of a single photon, and

$$\frac{dI^{\rm pol}_{\rm QED}(\omega')}{d\omega'} = C_{fi}\frac{dI_{\rm cl}\left(\frac{\omega'}{C_{fi}}\right)}{d\omega'} = \frac{C_{fi}I_{\rm cl}}{\omega_c}Q_{\rm cl}\left(\frac{r}{C_{fi}}\right). \quad (35)$$

Within the framework of QED, the electron possesses not only an electric charge, but also a magnetic moment associated with its spin. Usually the spin is assumed to be depolarized (as is done in Ref. 15), and, accordingly, a depolarized contribution to the emission appears

$$\frac{dI^{\rm depol}_{\rm QED}}{d\omega'} = \frac{I_{\rm cl}(\tau)}{\omega_c}\frac{9\sqrt{3}}{8\pi}(1-C_{fi})^2\frac{r}{C_{fi}}K_{2/3}\left(\frac{r}{C_{fi}}\right). \quad (36)$$

Thus, the QED effect in the emission from an electron in a strong field reduces to a downshift in frequency accompanied by an extra contribution from the magnetic moment of electron. The universal emission spectrum in QED-strong fields is given by the sum of Eqs. (35) and (36),

$$\frac{dI_{\rm QED}}{d\omega'} = \frac{I_{\rm cl}}{\omega_c}q(\chi)Q_{\rm QED}(r,\chi), \quad I_{\rm QED} = I_{\rm cl}q(\chi),$$

where $Q_{\rm QED} = Q'_{\rm QED}/q$ is the unity normalized spectrum, $q(\chi) = \int_0^\infty Q'_{\rm QED}(r,\chi)dr \le 1$ is the normalization parameter, and the spectrum before normalization is

$$Q'_{\rm QED}(r,\chi) = \frac{9\sqrt{3}}{8\pi}r\left[\int_{r_\chi}^{\infty}K_{5/3}(r')dr' + \chi^2 r r_\chi K_{2/3}(r_\chi)\right],$$

and $r_\chi = r/(1-\chi r)$. The graph of $I_{\rm QED}$ is shown in Fig. 3.

2. Equation for electron motion: Accounting the radiation back-reaction

As long as QED effects modify emission,

$$Q_{\rm cl}(r) \to Q_{\rm QED}(r,\chi), \quad I_{\rm cl} \to I_{\rm QED}, \quad (37)$$

the radiation back-reaction needs to be revised accordingly. In Refs. 3 and 19, it is noted that QED is not compatible with the traditional approach to the radiation force in classical electrodynamics, while Eqs. (15) and (16) may be employed at finite value of χ on substituting $I_{\rm QED}$ for $I_{\rm cl}$. Alternatively, within the framework of QED, the radiation back-reaction may be found by integrating the 4-momentum carried away with the emitted photons and that absorbed

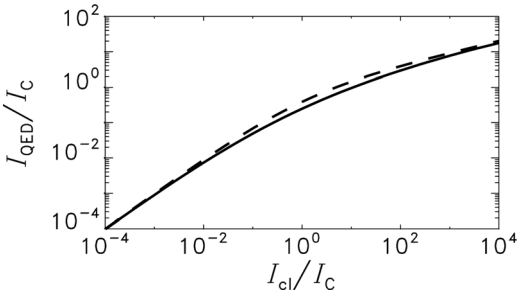

FIG. 3. Emitted radiation power in the QED approach *vs* classical (solid), an interpolation formula $I_{\rm QED} = I_{\rm cl}/(1+1.04\sqrt{I_{\rm cl}/I_C})^{4/3}$ (dashed). Here, $I_C = I_{\rm cl}/\chi^2$.

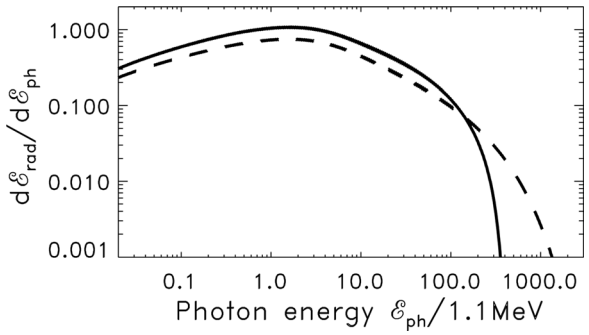

FIG. 4. The emission spectrum for 600 MeV electrons interacting with 30-fs laser pulses of intensity $2 \cdot 10^{22}$ W/cm^2 and wavelength $\lambda = 0.8$ μm, with (solid) and without (dashed) accounting for the QED effects. The QED effects cut off the high-energy part of the emission, though the reduction in the radiation back-reaction elevates the low-energy emission.

from the external electromagnetic field in the course of emission. For a 1D wave field, this procedure gives the following equation (see Ref. 15):

$$\frac{dp^\alpha}{d\tau} = \frac{f^\alpha_{Le}}{m_e c} + \frac{I_{\rm QED}}{m_e c^2}\left[\frac{k^\alpha}{(k\cdot p)} - p^\alpha\right], \tag{38}$$

and in such a field, $F^{\alpha\beta}F_{\beta\mu}p^\mu/\left(p_\nu F^{\nu\beta}F_{\beta\mu}p^\mu\right) = k^\alpha/(k\cdot p)$, where k^α is the wave 4-vector. Eq. (38) coincides with Eqs. (15) and (16), in which the substitutions of Eq. (37) are made. Similarly, the three-vector formulation for $\bar{\mathbf{u}}$ is applicable to the 1D wave field, if the substitution is done as follows:

$$\tau_0 \to \tau_0 \frac{I_{\rm QED}}{I_{\rm cl}} = \tau_0 q(\chi). \tag{39}$$

Although this approach is derived for the 1D field, we may apply it to an arbitrary 3D focused field. An argument in favor of this generalization is that the property of a 1D wave, $(k\cdot k) = 0$, which is used while deriving Eq. (38), holds as an approximation for any field. Indeed on calculating the 4-square of $F^{\alpha\beta}F_{\beta\mu}p^\mu/\left(p_\nu F^{\nu\beta}F_{\beta\mu}p^\mu\right)$, which 4-square is similar to $(k\cdot k)/(k\cdot p)^2$, we find

$$\frac{p\cdot F^4\cdot p}{(p\cdot F^2\cdot p)^2} = \frac{9}{4}\chi^{-2}\frac{E^2-B^2}{E_S^2} + \frac{81}{16}\chi^{-4}\frac{(\mathbf{E}\cdot\mathbf{B})^2}{E_S^4} \ll 1,$$

which holds at $\chi \geq 1$ according to inequality (6).

Another criterion which should be checked at $\chi \geq 1$ is the requirement for the difference, $(1-u^2) \propto \chi^2$, as in Eq. (21) to be small. Applying the substitution in Eqs. (39) to (21), we find that $(1-u^2) \leq 2\cdot 10^{-6}$, reaching its maximal value at $\chi \sim 3.4$. This "error" is negligible, even if one assumes, than any theory allowing $u^2 \neq 1$, is erroneous.

B. Analytical result

In Fig. 4, we show the emission spectrum for an electron interacting with a laser pulse (see Ref. 15 for detail). We see that the QED effects essentially modify the spectrum even with laser intensities which are already achieved.

C. Numerical model

As long as the QED spectrum of emission depends on χ, the bins for collecting the radiation energy should be refined, $\mathcal{E}_{{\rm rad}\,ijkl}(\bar{\omega}_i, \mathbf{n}_{jk}, \chi_l)$. Once, for a given electron (or positron), the parameter χ is calculated; the discrete value of χ_l should be found most close to χ. Then, parameter ε should be found following Eq. (39), $\varepsilon = q_l\tau_0\omega$, using pre-tabulated value, $q_l = q(\chi_l)$. Then, $\bar{\mathbf{u}}_e$ should be expressed in terms of ε and the radiated energy should be added to a proper energy bin,

$$\mathcal{E}_{{\rm rad}\,ijkl} \to \mathcal{E}_{{\rm rad}\,ijkl} + \frac{(\mathcal{E}_e^{(n+1/2)})^2(\mathbf{f}_{Le}\cdot\bar{\mathbf{u}}_e)\Delta t}{\omega_c N_{ppc}\Delta\log(\bar{\omega})\Delta\mathbf{n}_{jk}}.$$

While postprocessing the results, a convolution similar to Eq. (14) should be applied with χ_l-dependent spectra,

$$\frac{d\mathcal{E}_{\rm rad}(\omega',\mathbf{n})}{d\mathbf{n}d\omega'} = \mathcal{E}_0\sum_{\chi_l}\int Q_{\rm QED}\left(\frac{\omega'}{\bar{\omega}},\chi_l\right)\mathcal{E}_{{\rm rad}\,ijkl}d\log\bar{\omega}.$$

D. Simulation result

In a 1D simulation presented in Fig. 5(a), a linearly polarized laser pulse with a step-like profile having 2-λ front and amplitude $a = 300$ interacts with plasma of density $n_0 = 30n_{\rm cr}$ during 50 cycles. About half of laser energy is converted to high energy photons. The data for backscattered photons indicate that values of $\chi \approx 1$ are achieved. These values are reasonable, as the energies of electrons moving toward the pulse are as high as 180 MeV, and the field magnitude is intensified. One can see that ~65% of emitted photons exceed 10 MeV and that 96% are above 1 MeV. In simulation presented in Fig. 5(b) for $a = 600$ and $n_0 = 60n_{\rm cr}$, the value of χ exceeds one.

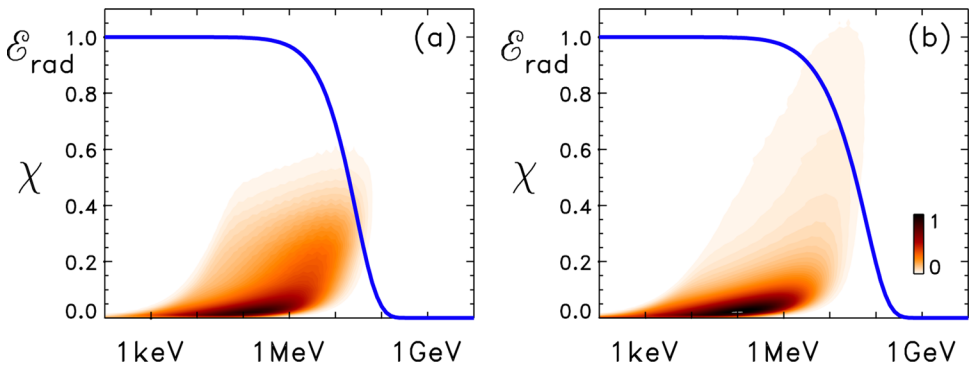

FIG. 5. (Color online) Backscattered light in simulations of the interaction of laser pulse of intensity (a) 2×10^{23} W/cm^2, (b) 8×10^{23} W/cm^2, with plasma of density (a) 6.5×10^{22} cm^{-3}, (b) 1.3×10^{23} cm^{-3}. For each χ_l (vertical axis), the convolution integral (the term in the above formula for convolution) is calculated and presented as a function of $\hbar\omega'$ (horizontal axis). The line shows the total emitted energy as a function of the cutoff photon energy (i.e., the integral spectrum).

IV. QED-STRONG FIELDS ($\chi \gg 1$)

A. Theoretical notes

In cases where $\chi \gg 1$, the photons cannot be considered as freely escaping from the plasma. Note that the processes of the emitted photon interaction with *the other electrons* may be evaluated in terms of the scattering cross-section, which is on the order of the Thomson cross-section, $\sigma_T \approx 6.65 \cdot 10^{-25}$ cm^2. Even in plasmas of high electron density, n_e, the scattering length, $(\sigma_T n_e)^{-1}$, is much longer than the spatial scale of laser-plasma interaction. As the laser intensity grows, the scattering efficiency slowly decreases, while the coincident process of the direct γ-photon absorption in strong field greatly increases. Therefore, one needs to solve the RTE in order to quantify this absorption.

This may be done using the Monte-Carlo method, in which the radiation field is evaluated statistically (see Ref. 22). Instead of the radiation energy density, the photon distribution function is introduced as follows:

$$f_\gamma(\mathbf{x}, \omega', \mathbf{n}) = \frac{\mathcal{I}(\mathbf{x}, \omega', \mathbf{n})}{m_e c^2 \omega'}. \tag{40}$$

Similar to the way that electron macroparticles represent the electron distribution function, photon marcoparticles may be employed to simulate the photon distribution function. To simulate emission, the photons are created with their momentum selected statistically. The photon propagation in the direction of $\mathbf{n}$ is simulated in the same way as for electrons. The absorption with the known probability is also simulated statistically.

Now we may split the radiation into one part, which may be treated in the way we followed so far (see Secs. II and III) and another, to be treated as Monte-Carlo photons. To do this, we choose a parameter $\chi^* \sim (0.05 - 1)$ and assume that: (1) an electron with $\chi \le \chi^*$ contributes only to $d\mathcal{E}_{\rm rad}/(d\omega' d\mathbf{n})$; while (2) for an electron with $\chi > \chi^*$, the *regular* spectrum of emission, $Q'_{\rm QED}(r, \chi)$ (which is normally truncated at $r = 1/\chi$), is now truncated at $r = \chi^*/\chi^2 < 1/\chi$, and the emission of photons with $\chi^*/\chi^2 \le r \le 1/\chi$, or, the same, $\frac{\chi^*}{\chi} \le \frac{\omega'}{\mathcal{E}} \le 1$, is treated statistically. The regular radiation loss rate as well as the contribution to the radiation force which is proportional to $-\mathbf{p} I_{\rm QED}$ should be both multiplied by a factor of $q_t(\chi)/q(\chi)$ at $\chi > \chi^*$, where the truncated spectrum integral equals $q_t(\chi) = \int_0^{\chi^*/\chi^2} Q'_{\rm QED}(r, \chi) dr$. The unity normalized truncated spectrum to be used in postprocessing is $Q_t(r, \chi) = \frac{q(\chi) Q_{\rm QED}(r, \chi)}{q_t(\chi)}$, $r < \chi^*/\chi^2$. The emission probability to be used at $\chi > \chi^*$, $r > \chi^*/\chi^2$ may be found in the supplement to Ref. 10,

$$dW_{e \to e,\gamma} = \frac{\kappa K_{2/3}(r_\chi) + \int_{r_\chi}^{\infty} K_{5/3}(r') dr'}{\pi \sqrt{3} \alpha \omega_{\rm au}} d\left(\frac{\omega'}{\mathcal{E}}\right) \frac{d(\omega t)}{\mathcal{E}},$$

where $r_\chi = \frac{\omega'/\mathcal{E}}{\chi(1-\omega'/\mathcal{E})}$, $\kappa = \frac{(\omega'/\mathcal{E})^2}{1-\omega'/\mathcal{E}}$, and for a 1D wave field, we use an equation, $\frac{d(\omega t)}{\sqrt{3}\alpha\omega_{\rm au}} = \frac{\sqrt{3}\alpha d\xi}{2\chi} \left|\frac{d\mathbf{a}}{d\xi}\right|$. If the emission probability is averaged over time or over an ensemble, we return to the above spectrum of emission, $\omega' m_e c^2 \langle dW_{e \to e,\gamma}/(drdt) \rangle = I_{\rm QED} Q_{\rm QED}(r, \chi)$. Here, we apply the formula, $\frac{1}{\sqrt{3}\alpha\omega_{\rm au}} = \frac{9\sqrt{3} I_{\rm QED}}{8\chi^2 q(\chi) \omega m_e c^2}$, which is also used in the numerical scheme.

B. Semi-analytical solution

In Ref. 10, we demonstrated that as long as the distribution functions, $f_{e,p,\gamma}$, for electrons, positrons, and photons in a 1D wave field are integrated over the transversal components of momentum, their evolution is described by simple kinetic equations with the collision integrals. We solved these equations numerically. The choice of initial conditions corresponds to the 46.6 GeV electron beam,[8] and the laser intensity of $J \approx 5 \cdot 10^{22}$ W/cm^2 for $\lambda = 0.8$ μm to be achieved soon. As long as the Monte-Carlo method is not used, the numerical results, such as the total pair production, may be used to benchmark the numerical scheme described here.

C. Numerical model

The modification of the numerical scheme as used in Sec. III is needed only for electrons and positrons with $\chi > \chi^*$. The radiation energy added to the proper energy bin is corrected at algorithm stage 2.4 as follows:

$$\mathcal{E}_{{\rm rad}\, ijkl} \to \mathcal{E}_{{\rm rad}\, ijkl} + \frac{q_t(\chi_l)}{q(\chi_l)} \frac{(\mathcal{E}_e^{(n+1/2)})^2 (\mathbf{f}_{Le} \cdot \bar{\mathbf{u}}_e) \Delta t}{\omega_c N_{ppc} \Delta \log(\bar{\omega}) \Delta \mathbf{n}_{jk}},$$

and the same correction factor is applied to the second term in braces at algorithm stage 2.5. After stage 2.5, a probable hard photon emission from the electron with $\chi > \chi^*$ is accounted, using the probability,

$$\frac{dW_{e \to e,\gamma}}{d(\omega'/\mathcal{E})} = \delta w\left(\frac{\omega'}{\mathcal{E}}, \chi\right), \quad \delta = \frac{\mathcal{E}_e^{(n+1/2)} (\mathbf{f}_{Le} \cdot \bar{\mathbf{u}}_e) \Delta t}{\chi^2},$$
$$w\left(\frac{\omega'}{\mathcal{E}}, \chi\right) = \frac{9\sqrt{3}}{8\pi q(\chi)} \left[\kappa K_{2/3}(r_\chi) + \int_{r_\chi}^{\infty} K_{5/3}(r') dr'\right].$$

The total probability of emission is given by a complete integral, $W_{e \to e,\gamma} = \delta \int_{\chi^*/\chi}^1 w\left(\frac{\omega'}{\mathcal{E}}, \chi\right) d\left(\frac{\omega'}{\mathcal{E}}\right)$. Both within the QED perturbation theory and within the Monte-Carlo scheme, $W_{e \to e,\gamma}$ is assumed to be less than one. The probability of no emission equals $1 - W_{e \to e,\gamma} \ge 0$. The partial probability, $W_{e \to e,\gamma}(\omega' < \omega'_0)$, for the emission with the photon energy not exceeding the given value, ω'_0, is given by the incomplete probability integral,

$$W_{e \to e,\gamma}(\omega' < \omega'_0) = \delta \int_{\chi^*/\chi}^{\omega'_0/\mathcal{E}} w\left(\frac{\omega'}{\mathcal{E}}, \chi\right) d\left(\frac{\omega'}{\mathcal{E}}\right).$$

Therefore, for given δ and χ and for a randomly generated number, $0 \le {\rm rnd} < 1$, one can solve $\omega'/\mathcal{E}$ from an integral equation as follows:

$$\int_{\chi^*/\chi}^{\omega'/\mathcal{E}} w(z, \chi) dz = \frac{\rm rnd}{\delta} \le \int_{\chi^*/\chi}^{1} w(z, \chi) dz, \tag{41}$$

if the gambled value of rnd does not exceed $W_{e\to e,\gamma}$: $0 \le \mathrm{rnd} \le W_{e\to e,\gamma}$. Otherwise (if $W_{e\to e,\gamma} < \mathrm{rnd} \le 1$), the extra emission does not occur. With calculated $\omega'/\mathcal{E}$, the emission is accounted for by creating a new photon macroparticle with momentum, $\mathbf{p}_e^{(n+1/2)}(\omega'/\mathcal{E})$ and the recoil of an electron is accounted for by reducing the ultimate electron momentum, $\mathbf{p}_e^{(n+1/2)} \to \mathbf{p}_e^{(n+1/2)}(1-(\omega'/\mathcal{E}))$.

1. Photon propagation and absorption

The new element of the numerical scheme is the photon macroparticle, which simulates $(n_{\mathrm{cr}}\Delta V)/N_{ppc}$ real photons. Its propagation with dimensionless velocity equal to $\mathbf{n}$ is treated in the same way as for electrons and ions.

If the photon escapes the computational domain, its energy should be accounted for while calculating the total emission from plasma. For this purpose, we introduce the energy bins, $\mathcal{E}^{(tot)}_{\mathrm{rad}\,ijk}(\log(\omega')_i, \theta_j, \varphi_k)$, such that the logarithmic equally spaced grid for the photon energy, $\log(\omega')_i$, and the polar angle grid coincide with those introduced above. The contribution from the escaping photon with total energy, $\omega' m_e c^2 n_{\mathrm{cr}}\Delta V/N_{ppc}$, should be added to the bin with the closest $\log(\omega')_i$, θ_j, φ_k, with the macroparticle energy being converted to the spectral energy density by dividing by $\Delta\omega' = \omega'\Delta\log(\omega')$,

$$\mathcal{E}^{(tot)}_{\mathrm{rad}\,ijk} \to \mathcal{E}^{(tot)}_{\mathrm{rad}\,ijk} + \frac{m_e c^2 (n_{\mathrm{cr}}\Delta V)}{N_{ppc}\Delta\log(\omega')}.$$

The photon absorption with electron-positron-pair creation is gambled in the same way as the emission. Other absorption mechanisms may be also included. In postprocessing the simulation results, the softer γ-photon emission should be added to the total radiation spectrum,

$$\frac{d\mathcal{E}_{\mathrm{rad}}(\omega',\mathbf{n})}{d\mathbf{n}d\omega'} = \mathcal{E}^{(tot)}_{\mathrm{rad}\,ijk} + m_e c^2 (n_{\mathrm{cr}}\Delta V) \times \sum_{\chi_l}\int Q_t\left(\frac{\omega'}{\bar{\omega}},\chi_l\right)\mathcal{E}_{\mathrm{rad}\,ijkl} d\log\bar{\omega}\,.$$

D. Simulation result

Repeating the test simulation as described in Sec. III D and applying the Monte-Carlo scheme at $\chi > \chi^* = 0.1$, and without photon absorption, we notice only an increase in the fluctuations of the high-energy portion of the radiation spectrum. In this region, the photons are statistically underrepresented, the number of particles per $\Delta\log(\omega')$ being small.

V. CONCLUSION

Thus, the range of field intensities which may be simulated with good accuracy using the described tools is now extended towards the intensities as high as $(2-3)\cdot 10^{23}$ W/cm^2. In such fields, which are typical for the radiation-dominated regime of the laser-plasma interaction, the suggested scheme is validated against a semi-analytical solution. Different versions of the equation of the emitting particle motion are compared and their proximity is demonstrated.

Extension of the model for moderately QED-strong fields can be easily incorporated into the scheme. The efficiency degradation compared to the standard PIC scheme is as low as 15%. The emission spectra are substantially modified by QED effects and simulation results for a realistic laser-plasma interaction are provided.

Regarding the QED-strong field of the laser-plasma interaction, the Monte-Carlo approach at large χ, appears to be extremely challenging and computationally intense (although, in principle, such simulations are doable—see Ref. 23). Roughly, for each electron (or positron) particle, one needs to trace about ten high-energy photon particles, potentially convertible to electron-positron pairs. This high photon-to-electron number ratio is caused by a comparatively low photon absorption probability, which is much lower than the photon emission probability. Full 3D simulation of the radiation transport (especially for such a nontrivial mechanism of absorption as we use here) is on a frontier of computational physics and it may be only achievable with forthcoming exa-flop-class supercomputers.

[1] V. Yanovsky, V. Chvykov, G. Kalinchenko, P. Rousseau, T. Planchon, T. Matsuoka, A. Maksimchuk, J. Nees, G. Cheriaux, G. Mourou, and K. Krushelnick, Opt. Express **16**, 2109 (2008).
[2] See http://eli-laser.eu/ for the Extreme Light Infrastructure European project; E. Gerstner, Nature **446**, 16 (2007).
[3] I. V. Sokolov, N. M. Naumova, J. A. Nees, G. A. Mourou, and V. P. Yanovsky, Phys. Plasmas **16**, 093115 (2009).
[4] J. Koga, T. Zh. Esirkepov, and S. V. Bulanov, Phys. Plasmas **12**, 093106 (2005).
[5] A. Zhidkov, J. Koga, A. Sasaki, and M. Uesaka, Phys. Rev. Lett. **88**, 185002 (2002); Y. Y. Lau, F. He, D. P. Umstadter, and R. Kowalczyk, Phys. Plasmas **10**, 2155 (2003); F. He, Y. Y. Lau, D. P. Umstadter, and R. Kowalczyk, Phys. Rev. Lett. **90**, 055002 (2003); S. V. Bulanov, T. Esirkepov, J. Koga, and T. Tajima, Plasma Phys. Rep. **30**, 196 (2004); N. M. Naumova, J. A. Nees, I. V. Sokolov, B. Hou, and G. A. Mourou, Phys. Rev. Lett. **92**, 063902 (2004); N. Naumova, I. Sokolov, J. Nees, A. Maksimchuk, V. Yanovsky, and G. Mourou, Phys. Rev. Lett. **93**, 195003 (2004); J. Nees, N. Naumova, E. Power, V. Yanovsky, I. Sokolov, A. Maksimchuk, S. Bahk, V. Chvykov, G. Kalintchenko, B. Hou, and G. Mourou, J. Mod. Optics **52**, 305 (2005); N. M. Naumova, J. A. Nees and G. A. Mourou, Phys. Plasmas **12**, 056707 (2005).
[6] N. Naumova, T. Schlegel, V. T. Tikhonchuk, C. Labaune, I. V. Sokolov, and G. Mourou, Phys. Rev. Lett. **102**, 025002 (2009); T. Schlegel, N. Naumova, V. T. Tikhonchuk, C. Labaune, I. V. Sokolov, and G. Mourou, Phys. Plasmas **16**, 083103 (2009).
[7] J. Schwinger, Phys. Rev. **82**, 664 (1951); E. Brezin and C. Itzykson, Phys. Rev. D **2**, 1191 (1970).
[8] C. Bamber, S. J. Boege, T. Koffas, T. Kotseroglou, A. C. Melissinos, D. D. Meyerhofer, D. A. Reis, W. Ragg, C. Bula, K. T. McDonald, E. J. Prebys, D. L. Burke, R. C. Field, G. Horton-Smith, J. E. Spencer, D. Walz, S. C. Berridge, W. M. Bugg, K. Shmakov, and A. W. Weidemann, Phys. Rev. D **60**, 092004 (1999); M. Marklund and P. K. Shukla, Rev. Mod. Phys. **78**, 591 (2006); Y. I. Salamin, S. X. Hu, K. Z. Hatsagortsyan, and C. H. Keitel, Phys. Rep. **427**, 41 (2006); A. M. Fedotov, N. B. Narozhny, G. Mourou, and G. Korn, Phys. Rev. Lett. **105**, 080402 (2010).
[9] A. R. Bell and J. G. Kirk, Phys. Rev. Lett. **101**, 200403 (2008).
[10] I. V. Sokolov, N. M. Naumova, J. A. Nees, and G. A. Mourou, Phys. Rev. Lett. **105**, 195005 (2010).
[11] L. D. Landau and E. M. Lifshits, *The Classical Theory of Fields* (Pergamon, New York, 1994).
[12] J. D. Jackson, *Classical Electrodynamics* (Wiley, New York, 1999).
[13] A. Rousse, K. Ta Phuoc, R. Shah, A. Pukhov, E. Lefebvre, V. Malka, S. Kiselev, F. Burgy, J.-P. Rousseau, D. Umstadter, and D. Hulin, Phys. Rev. Lett. **93**, 135005 (2004); S. Kiselev, A. Pukhov, and I. Kostyukov, Phys. Rev. Lett. **93**, 135004 (2004).
[14] S. Kneip, S. R. Nagel, C. Palmer, C. Bellei, J. Schreiber, S. P. D. Mangles, Z. Najmudin, C. McGuffey, C. Huntington, F. Dollar, T. Matsuoka,

V. Chvykov, G. Kalintchenko, V. Yanovsky, A. Maksimchuk, K. Ta Phuoc, and K. Krushelnick, Proc. SPIE **7359**, 73590T (2009).
[15]I. V. Sokolov, J. A. Nees, V. P. Yanovsky, N. M. Naumova, and G. A. Mourou, Phys. Rev. E **81**, 036412 (2010).
[16]J. L. Martins, S. F. Martins, R. A. Fonseca, and L. O. Silva, Proc. SPIE **7359**, 73590V (2009).
[17]A. G. R. Thomas, Phys. Rev. ST Accel. Beams **13**, 020702 (2010).
[18]Y. B. Zel'dovich and Y. P. Raizer, *Physics of Shock Waves and High-Temperature Hydrodynamic Phenomena* (Academic, London, 1967).
[19]I. V. Sokolov, JETP **109**, 207 (2009).
[20]I. V. Sokolov, N. M. Naumova, J. A. Nees, V. P. Yanovsky, and G. A. Mourou, AIP Conf. Proc. **1228**, 305 (2010).
[21]C. K. Birdsall and A. B. Langdon, *Plasma Physics via Computer Simulation* (McGraw-Hill, New York, 1985).
[22]S. Nayakshin, S. H. Cha, and A. Hobbs, MNRAS **397**, 1314 (2009); A. Maselli, A. Ferrara, and S. Gallerani, MNRAS **395**, 1925 (2009); S. Baek, P. Di Matteo, B. Semelin, F. Combes, and Y. Revaz, Astron. Astrophys. **495**, 389 (2009).
[23]E. N. Nerush, I. Y. Kostyukov, A. M. Fedotov, N. B. Narozhny, N. V. Elkina, and H. Ruhl, Phys. Rev. Lett. **106**, 035001 (2011).